Magnetic structure of DyN: A ^{161}Dy Mössbauer study

Jacob P. Evans,[1,*] Glen A. Stewart,[2] J. M. Cadogan,[2] Wayne D. Hutchison,[2] Emma E. Mitchell,[3] and James E. Downes[1]

[1]*MQ Photonics Research Centre, Department of Physics and Astronomy, Macquarie University, New South Wales 2109, Australia*

[2]*School of Physical, Environmental, and Mathematical Sciences, University of New South Wales, Australian Defence Force Academy, Canberra BC, Australian Capital Territory 2600, Australia*

[3]*Materials Science & Engineering, Commonwealth Scientific and Industrial Research Organization, New South Wales 2070, Australia*

(Received 17 July 2016; revised manuscript received 12 January 2017; published 27 February 2017)

Conventional magnetometry yields a low temperature bulk magnetic moment of about 4 μ_B/Dy^{3+} in an applied field of $\mu_0 H = 9$ T for thin and thick dysprosium nitride (DyN) films. This is significantly lower than the maximum possible value of 10 μ_B/Dy^{3+}. Ion-assisted deposition was used to grow 5.7-μm-thick rare earth nitride DyN films on organic Kapton® substrates. ^{161}Dy Mössbauer spectroscopy (with its time scale on the order of nanoseconds) indicates thermal relaxation between fully stretched $\pm 10\,\mu_B$ levels of a low-lying Kramers doublet, which is inconsistent with the Dy^{3+} site's ideal cubic symmetry. However, a small tetragonal distortion [$\epsilon \approx -0.024(10)$] observed using x-ray powder diffraction is compatible with an additional rank 2 crystal field term, $B_2^0 \approx -1.0(4)$ K, approaching the magnitude estimated to bring this about. The observed magnetic behavior can then be described using a two-level, molecular field model with θ_C set to ≈6–8 K, which is substantially smaller than the accepted ordering temperature of $T_C \approx 17$–26 K.

DOI: 10.1103/PhysRevB.95.054431

I. INTRODUCTION

The rare-earth mononitride (REN) series has attracted considerable research interest [1] because of the coexistence of semiconducting and ferromagnetic properties, a feature ideal for spintronic devices.

Dysprosium nitride (DyN) is a promising candidate whose electronic structure is relatively well understood. However, its magnetic structure has received little attention until recently. The conducting state of DyN was an area of contention when first investigated in the 1960s [2,3]. However, recent advances in growth techniques have conclusively shown DyN is a semiconductor [4]. A detailed study of the band structure of DyN was presented by Preston *et al.* [4].

Bulk DyN forms with the face-centered cubic, rock salt structure (space group $Fm\bar{3}m$ #225 with $Z = 4$) and a room temperature lattice parameter of $a = 4.901$ Å [5]. It orders ferromagnetically with experimental Curie temperatures reported in the range of $T_C = 17$–26 K [1]. According to the early neutron powder diffraction paper of Child *et al.* [6], the Dy moments align in the [100] direction.

The results of recent investigations are summarized in Table I. Nakagawa *et al.* [5] employed Arrott plots to determine a value of $T_C = 21$ K for a bulk DyN specimen. However, for a thin film DyN (sapphire) specimen, Preston *et al.* [4] identified $T_C = 25$ K as the temperature at which temperature dependent, field-cooled (FC) and zero-field-cooled (ZFC) magnetizations were observed to diverge. These values sit in the middle and at the upper end of the 17–26 K range, respectively.

There is considerably more variation (Table I) in the reported Dy^{3+} magnetic moment obtained from the low temperature saturation magnetization, which ranges from 7.0 μ_B/Dy for a bulk DyN specimen [5] down to 3.95 μ_B/Dy determined for a thin film DyN (sapphire) specimen using polarized neutron reflectometry [7]. One reason for the scatter in these values could be the accuracy to which the thickness of the DyN thin films is determined. Another could be due to the inclination of DyN thin films to oxidize. A successful extraction of the bulk magnetization (expressed as mean moment per Dy^{3+} ion) from the measured bulk magnetic moment relies on precise knowledge of the number of Dy atoms in the sample. In two of the cases reported in Table I, the film thickness was not provided. Nevertheless, given that the maximum possible magnetization is equal to the free-ion moment of $\mu_{FI} = g_J \times J = \frac{4}{3} \times \frac{15}{2} = 10\,\mu_B$, it is evident that mechanisms such as the crystal field (CF) interaction, noncollinear alignment of the magnetic moments, or strong magnetocrystalline anisotropy are involved.

The objective of our paper was therefore to investigate the local magnetic moment at the Dy^{3+} site in DyN in the context of the local CF interaction using conventional magnetometry in combination with ^{161}Dy Mössbauer spectroscopy.

II. EXPERIMENTAL DETAILS

The DyN samples were prepared using ion-assisted deposition (IAD) at Macquarie University (New South Wales, Australia). An important constraint concerning the preparation of the DyN films was that the ^{161}Dy Mössbauer signal needed to be maximized. Focusing on the most intense absorption line of the expected magnetically split spectrum, the thickness optimization approach described by Moolenaar [8] yields an optimum thickness of 35 mg DyN/cm^2, which corresponds to a film thickness of 36 μm. The film deposition technique currently employed for the preparation of thin film (10–200 nm) DyN on 10×10 mm^2 sapphire substrates was therefore modified for the production of thicker layers (≈4–7 μm DyN) on less absorbent, larger surface area (2.54 cm diameter) Kapton® substrates. Five of these DyN discs could then be stacked to achieve the desired DyN absorber thickness. Although these films were substantially thicker than rare earth nitride films investigated elsewhere, it was anticipated that their properties should be driven by the deposition process rather than by the substrate or internal strain. At the lower end

*Corresponding author: Jacob.evans@students.mq.edu.au

TABLE I. Overview of recent magnetization results for DyN.

Sample	a (Å)	T_C (K)	Magnetization			Reference
			M (μ_B/Dy)	T (K)	μ_0H (T)[a]	
Bulk	4.901	21[b]	7.0	5	5	[5]
Film[c]		25[d]	≈5.5[e]	5	6	[4]
Film (100 nm)			6.0–6.5[e]	2	2.5	[13]
Film (15–40 nm)	4.895		3.95[f]	5	1	[7]
Film (5.7 μm)			3.9[e]	2	9	This paper

[a]Applied magnetic field at which the magnetization was determined.
[b]Based on Arrott plots.
[c]Perhaps 200 nm (based on specimen preparation details referred to in Refs. [13] and [14]).
[d]Based on ZFC/FC magnetization divergence.
[e]Strongly dependent on precision to which the film thickness can be determined.
[f]Polarized neutron reflection (PNR) determination of local moment.

of the thickness range, it was already observed by Cortie *et al.* [7] that DyN films of thickness 200 nm exhibited the same properties as those of only 20 nm.

The Kapton substrates were cleaned using acetone and pressurized nitrogen before being placed in an oxygen plasma cleaner. The Kapton was then mounted on the substrate holder, and the IAD system was baked for about 8 h (reaching pressures of $\approx 10^{-7}$ torr). The DyN sample layer was grown at a rate of 0.05–0.3 nm/s using ion-assisted deposition with a typical activated N_2 pressure of about 6×10^{-4} torr. The substrate was measured to reach temperatures of 120 °C due to the heat inside the chamber and associated with the depositing metal. To achieve the desired thickness, the samples were grown over two depositions. The chamber was brought back up to pressure and restocked with Dy metal before being evacuated and baked again. A capping layer was not deposited (due to strain concerns). The resultant samples were placed under vacuum as soon as possible after deposition. After the measurements, no evidence of surface oxidation was observed. The thicknesses of the deposited DyN layer and Kapton substrate were measured at 5.7(3) and 82.0(2) μm, respectively, by using an ion beam to cut a cross section that was then analyzed using a scanning electron microscope (SEM), as shown in Fig. 1.

To understand the crystal structure, x-ray diffraction (XRD) patterns were recorded using a PANalytical X'Pert Pro MPD diffractometer with Cu-K_α radiation ($\lambda = 0.154$ nm) and analyzed using the FullProf/WinPLOTR programs [9,10]. Low temperature magnetization measurements were performed on a superconducting quantum interference device (SQUID) magnetometer and a Quantum Design physical property measurement system (PPMS) operating down to 2 K.

The ^{161}Dy 25.7 keV Mössbauer spectra were collected in transmission mode at University of New South Wales (UNSW) Canberra using a room temperature ^{161}Tb : $^{161}GdF_3$ source mounted on a sinusoidal motion drive. The source was activated at Australia's Open Pool Australian Lightwater (OPAL) reactor ($3d$, 10^{13} n/cm^2 per second) according to the reaction

$$^{160}\mathrm{Gd}(97\%\,\mathrm{enr}) \xrightarrow{n,\gamma} {}^{161}\mathrm{Gd}(T_{1/2} = 3.7\,\mathrm{m}) \xrightarrow{\beta} {}^{161}\mathrm{Tb}(T_{1/2} = 6.9\,\mathrm{d})$$

The stacked DyN (Kapton) absorbers were sandwiched between beryllium discs and cooled in a liquid helium cryostat. A 48-μm-thick reference Dy metal foil (≈41 mgDy/cm^2) was employed in separate measurements to calibrate the drive velocity. The transmitted 25.7 keV gamma photons were counted using an argon gas–filled proportional counter.

III. EXPERIMENTAL RESULTS

A. Structural characterization

A typical XRD pattern for the DyN films grown on Kapton is shown in Fig. 2. From the dominance of the (111) and

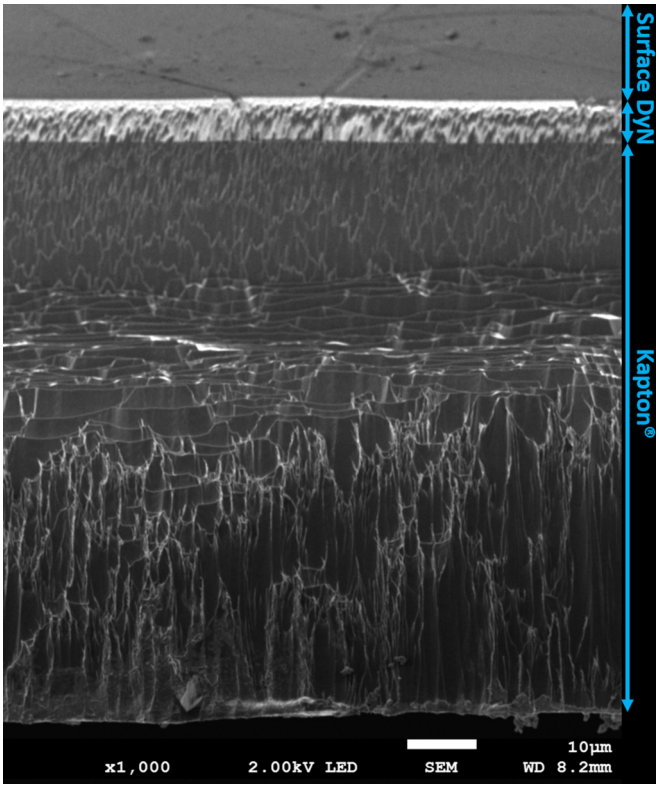

FIG. 1. SEM cross-sectional image of one of the DyN specimens. The specimen was cut using an argon ion beam, which is responsible for the streaks throughout. It appears the Kapton was not cut straight through, but instead a step (or ledge) occurs approximately half way down. The illuminated section at the top is the DyN layer. Its thickness is measured at 5.7(3) μm. It also appears there is a tapered ledge at the surface, indicated by the cracks through the sample.

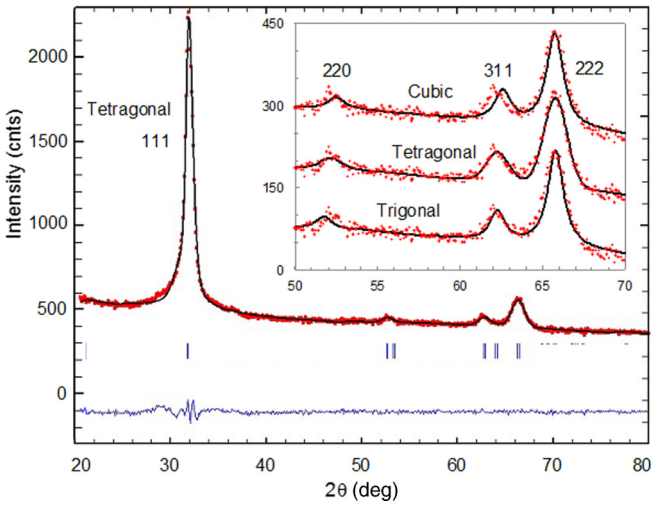

FIG. 2. X-ray powder diffraction pattern recorded with Cu Kα radiation for a DyN (Kapton) film at room temperature and fitted using the Le Bail approach. A comparison of fits based on three different crystal structures is presented in the insert: face-centered cubic (Cubic), face-centered tetragonal (Tetragonal), and primitive trigonal (Trigonal). The main plot is the full tetragonal fit with lattice parameters as detailed in the text. The vertical blue tick bars represent the allowed reflections, and the difference between the experimental data and the Le Bail fit is provided by the blue line.

(222) reflections it is clear that there is a strong preferred alignment of the DyN grains with their [111] axes directed perpendicular to the film surface. There are two additional low intensity peaks located at 2θ values close to those expected for the (220) and (311) reflections that are allowed for an ideal face-centered cubic DyN structure. Most often, it is only the (111) reflection that is observed for thin ($\leqslant$200 nm) DyN films grown on Al_2O_3 at low temperatures. We attribute the enhancement of the (222) peak in this present paper to the increased thickness and associated x-ray path length, and the emergence of the (220) and (311) peaks to the curvature of the Kapton substrate. The full diffraction pattern was analyzed in terms of the expected face-centered cubic structure using the Le Bail approach [11], where the intensities of the reflections are allowed to vary independently in the absence of detailed knowledge of the atomic position parameters. However, it was not possible to match simultaneously the positions of all four reflections. This is demonstrated by the expanded view of the fitted theory curve (labeled "Cubic") that is shown at the top of the insert in Fig. 2. Also shown in the insert are fits based on a face-centered tetragonal structure (Tetragonal) and a primitive trigonal structure (Trigonal). The closest match to the peak positions was achieved using the tetragonal structure with lattice parameters of $a = 4.920(16)$Å and $c = 4.804(30)$Å, corresponding to a small tetragonal compression (along one of the [100] directions) with $c = (1 + \epsilon)a$ and $\epsilon \approx -0.024(10)$ or $-2.4(1.0)\%$. The full tetragonal fit is provided as the main component of Fig. 2. However, it is important to recognize that this conclusion is based on fits to the peak positions alone and is subject to considerable uncertainty. Because of the nanocrystallinity of the film, the splitting of the (220) and (311) reflections that is expected for tetragonal distortion is comparable to the full width at half maximum (FWHM) line width and therefore not easily resolved. Using the Scherrer approach [12], a comparison of the fitted FWHM line widths for thick-film DyN with that recorded for crystalline Al_2O_3 under the same conditions leads to a minimum DyN crystallite dimension of 7–8 nm. No study has focused on the crystalline structure of REN thin films. It has been assumed that they retain the face-centered cubic structure of their bulk counterparts. On the basis of the above considerations, it is proposed that more detailed crystallographic studies need to be undertaken.

B. Magnetic measurements

Low-temperature magnetization curves were recorded on the Quantum Design PPMS system for an approximately square piece (surface area 22.84 mm^2) of DyN cut from one of the discs prepared for Mössbauer spectroscopy. The data are shown in Fig. 3(a) with green and red symbols used for $T = 2$ and 5 K, respectively. The increasing (decreasing) applied field condition is represented by solid (open) symbols. The derivation of the bulk magnetization as a mean moment per Dy^{3+} ion was based on a DyN film thickness of 5.7 μm, assuming a continuous bulk structure. The solid black symbols represent additional measurements recorded on the SQUID magnetometer at 5 K for a second sample of uncertain DyN mass and scaled to the corresponding PPMS data at $\mu_0 H = 7$ T. The two sets of magnetization curves are then observed to be in excellent agreement. As expected, the magnetization increases most rapidly with applied field for $T = 2$ K and $H \parallel$ surface. Based on these data, the saturated, low temperature magnetization is estimated at $M_{sat} \approx 3.9\,\mu_B$/Dy (Table I), in agreement with DyN thin films grown on Al_2O_3 [7].

The SQUID magnetometer was also used to record the mass susceptibility $\chi(T) = M(T)/H$ for the second sample. The reciprocal susceptibility χ^{-1} is plotted in Fig. 3(b) as a function of temperature. The data are observed to exhibit linear behavior above $T \approx 50$ K. For these higher temperatures, the Curie-Weiss law $\chi^{-1} = (T-\theta_C)/C$ was fitted to the data, which were then scaled so that the fitted gradient corresponded to the expected effective moment of $\mu_{eff} = g_J\sqrt{J(J+1)} = \frac{4}{3}\sqrt{\frac{15}{2}(\frac{15}{2}+1)} \approx 10.56\,\mu_B/Dy^{3+}$. At lower temperatures, the effects of the CF becomes important and causes deviations from the Curie-Weiss law. However, there is a further low temperature region ($25 < T < 40$ K) over which there is linear temperature dependence. Fitting these data to the same Curie-Weiss law yielded an effective moment of about $14.7\,\mu_B/Dy^{3+}$ and a temperature intercept of $\theta_C \approx 17$ K, lying at the lower end of the 17–26 K range of ordering temperatures reported in the literature [1]. The influence of the CF on the ground state doublet of the Dy^{3+} CF scheme is discussed in more detail in Sec. IV.

C. ^{161}Dy Mössbauer spectroscopy

The ^{161}Dy Mössbauer spectra recorded at 5 K for the reference Dy metal absorber and DyN are shown at the bottom of Fig. 4, and the fitted hyperfine interaction parameters are presented in the first two rows of Table II.

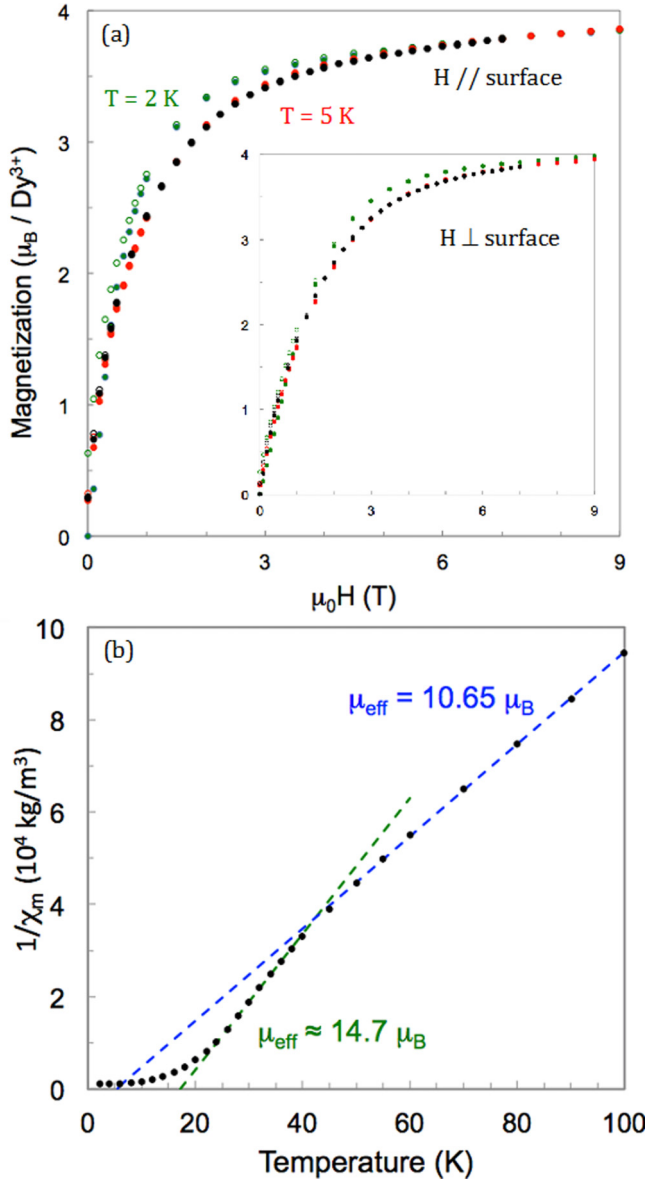

FIG. 3. (a) Low temperature PPMS magnetization curves recorded for a single DyN (Kapton) specimen of surface area 22.84 mm^2. The data for increasing and decreasing applied field conditions are distinguished by solid and open symbols, respectively. The derivation of the magnetization as a mean moment per Dy^{3+} ion was based on a DyN film thickness of 5.7 μm and assumed a continuous bulk structure. The magnetization increases most rapidly for $T = 2$ K and H // surface. The black data points represent SQUID data recorded at 5 K for a second sample of uncertain DyN mass and scaled to the corresponding PPMS data for $\mu_0 H = 7$ T. (b) Inverse magnetic susceptibility SQUID data (solid black circles) obtained from FC ($\mu_0 H = 0.01$ T) magnetization measurements for the second DyN specimen. The blue and green broken lines represent, respectively, the high temperature and low temperature Curie-Weiss fits. The experimental data were scaled to give the theoretical high temperature effective moment of $\mu_{\text{eff}} = 10.65\,\mu_B/Dy^{3+}$ ion.

The Dy metal spectrum was fitted using a simple coaxial hyperfine Hamiltonian of the form

$$\mathcal{H}_{\text{nucl}} = \mathcal{H}_{\text{mag}} + \mathcal{H}_{\text{quad}} = a\hat{I}_z + P'\left[3\hat{I}_z^2 - I(I+1)\right] \qquad (1)$$

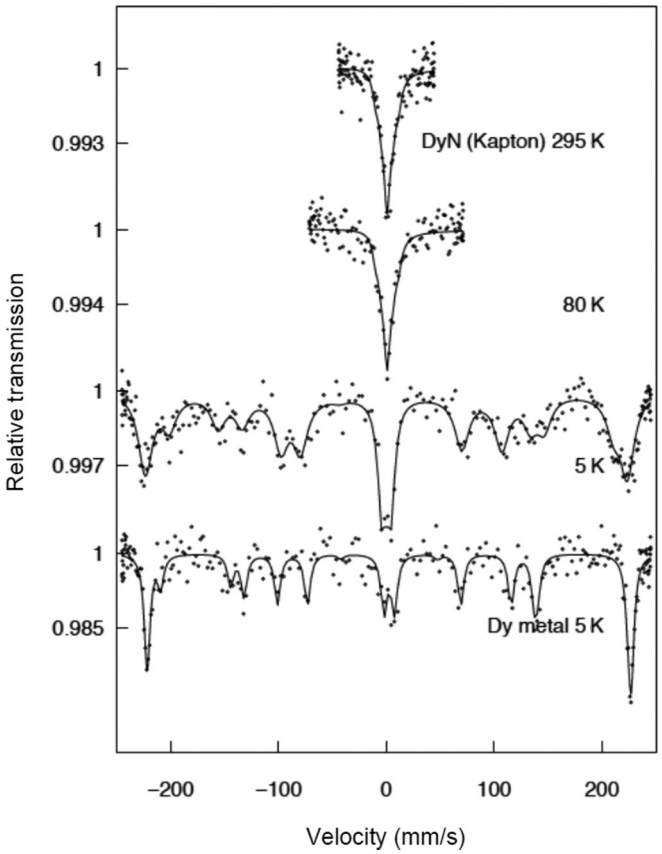

FIG. 4. ^{161}Dy Mossbauer spectra recorded for a reference specimen of Dy metal and a stack of five DyN (Kapton) films estimated to give a total thickness of $5 \times 5.7\,\mu\text{m} = 28.5\,\mu\text{m}$. The 5 K spectrum for DyN was analyzed in terms of a spin fluctuation model as described in the text.

for both the ground ($I_g = 5/2$) and excited ($I_e = 5/2$) nuclear levels of the $E1$, 25.7 keV Mössbauer transition. $a(I) = B_{\text{eff}}\mu(I)/I$ represents the nuclear Zeeman splitting and $P'(I)$ is a (first-order perturbation) quadrupole interaction term with the z axis defined as the direction of the magnetic hyperfine field B_{eff} [16]. From high precision nuclear magnetic resonance measurements, $a(I_g) = 830.3(5)$ MHz for Dy metal at 4.2 K [17,18], which converts to 40.132(3) mm/s in Mössbauer velocity units. This was used to calibrate the drive's maximum velocity at 245.05 mm/s.

By visual comparison, the spectrum of DyN differs from that of Dy metal in terms of the relative intensities of the 16 absorption lines and, in particular, the broader outer lines and sharper, more intense, central lines. This is typical of intermediate, spin-lattice relaxation (i.e., at a fluctuation rate comparable to the rate of Larmor precession of the ^{161}Dy nuclear moment about the magnetic hyperfine field). An informative example that is relevant to the present paper is provided by the ^{161}Dy Mössbauer investigation of Dy-Fe multilayer specimens reported by Tappert *et al.* [19]. In that article, simulated spectra are presented for a range of spin-lattice fluctuation rates and doublet splittings. The analysis was therefore carried out using the relaxation model of Nowik and Wickman [15], where spin-up and spin-down states of a low-lying electronic doublet (or pseudodoublet) are assumed to generate magnetic hyperfine fields of equal magnitude and

TABLE II. ^{161}Dy Mössbauer results for DyN: isomer shift δ, hyperfine interaction parameters $P(I_g)$ and $a(I_g)$, effective hyperfine field $B_{\rm eff}$, and the principal component of the electric field gradient V_{zz}. In the context of the relaxation model of Nowik and Wickman [15], Δ is the ground doublet splitting and τ is the fluctuation time between spin-up and spin-down states of the low-lying doublet.

	T (K)	δ[a] (mm/s)	τ (ns)	Δ (K)	$a(I_g)$ (mm/s)	$B_{\rm eff}$(T)	$P(I_g)$ (mm/s)	$V_{zz}(10^{21}\,{\rm V/m^2})$
Dy metal	5	2.7(2)			40.13(3)	567(3)	3.10(5)	42.3(1.0)
DyN[b]	5	0.8(2)	0.14(5)	13(2)	40.1(1)	567(4)	2.26(6)	30.9(1.1)
	80	0.8(2)					$\pm$0.92(10)[c]	$\pm$12.6(1.5)[c]
	295	1.0(2)					$\pm$1.0(1)[c]	$\pm$13.7(1.5)[c]

[a]With respect to GdF_3 at room temperature.
[b]Stack of 5 DyN (Kapton) films, each of estimated thickness 5.7 μm.
[c]Sign cannot be derived from spectrum analysis alone.

opposite sign at the ^{161}Dy nucleus. The key parameter is the fluctuation time, τ, the average interval for switches between the two states. A simplifying factor for the relaxation model fit was that the sample texture could be ignored. The absorption line intensities are well known to depend on the spatial average $\langle\cos^2\theta\rangle$ where θ is the angle between the incident γ-ray direction (the film-normal direction) and the direction of the hyperfine magnetic field (or local magnetization) at the Dy sites. However, in this instance, the [111] direction is aligned with the film normal, the local magnetization is aligned with the [100] direction, and the two directions subtend an angle of $\theta = 54.7^\circ$, thus making it indistinguishable from the case of random spin alignment where $\theta_{\rm ave} = \arccos\langle\cos^2\theta\rangle^{1/2}$ also equals the so-called "magic angle" of $\theta_{\rm ave} = 54.7^\circ$.

The fit to the 5 K spectrum for the DyN (Kapton) sample yielded a fluctuation time of $\tau = 0.14(5)$ ns and a doublet splitting of $\Delta = 13(2)$K. The isomer shift δ (measured relative to the room temperature GdF_3 source) is sensitive to the electron charge distribution at the nucleus and the large value of +2.7(2) mm/s observed for the Dy metal is due to the contribution from conduction electrons. The smaller isomer shift of +0.8(2) mm/s relative to GdF_3 fitted for DyN is therefore in keeping with its reported semiconductor properties [3,4]. This value is also close in value to the room temperature isomer shift of +0.85(8) mm/s re DyF_3 reported by Abele *et al.* [20] for a bulk DyN specimen prepared by nitrogen loading at 800 °C. However, the isomer shift for DyN may need to be adjusted to +1.25 mm/s when expressed relative to GdF_3 (based on a comparison of the isomer shift values of +3.1 mm/s re GdF_3 [21] and 2.7 mm/s re DyF_3 [22] quoted for Dy metal at 4.2 K).

Using the nuclear magnetic moment of $\mu(I_g) = 0.4803(25)\mu_{\rm N}$ [23], the value of $a(I_g) = 40.1(1)$ mm/s fitted to the DyN spectrum corresponds to an effective hyperfine field of $B_{\rm eff} = 567(4)$T and a Larmor precession period of 1.2 ns (approximately eight to nine times longer than the fitted mean spin fluctuation time of 0.14 ns). In other words, the spin fluctuation rate is within a factor of 10 of the Larmor precession frequency. Given the low Curie temperature of 17–26 K, extraionic hyperfine field contributions to $B_{\rm eff}$ are expected to be negligible. The hyperfine field is then proportional to the local expectation value of the $4f$ angular momentum according to

$$\frac{B_{\rm eff}}{B_{\rm FI}} \approx \frac{|\langle\pm|J_z|\pm\rangle|}{J} \qquad (2)$$

with a free-ion field of $B_{\rm FI}(Dy^{3+}) = 559.8$ T [24]. The fitted hyperfine field therefore corresponds to expectation values of $|\langle\pm|J_z|\pm\rangle| \approx 7.6$ and $|\langle\pm|\mu|\pm\rangle| = g_J|\langle\pm|J_z|\pm\rangle| = 10.1\,\mu_{\rm B}$, within 1% of the "fully stretched" values of $J = 15/2 = 7.5$ and $\mu_{\rm FI} = g_{\rm J}J = 4/3 \times 15/2 = 10\,\mu_{\rm B}$, respectively.

For Dy metal, the principal axis of the electric field gradient (efg) tensor is perpendicular to the direction of $B_{\rm eff}$ so that the P' term represents a first-order perturbation term (projected onto the $B_{\rm eff}$ axis) [16]. However, in the case of DyN, where the local magnetization is aligned with the fourfold symmetry [100] direction and the asymmetry parameter $\eta = \frac{V_{xx}-V_{yy}}{V_{zz}} = 0$, it can be expressed as

$$P' = \frac{eQV_{zz}}{4I(2I-1)} \qquad (3)$$

Using the electric quadrupole moment of $Q(I_g) = 2.507(20)$ b [23], the value of $P'(I_g) = 2.26\,(6)$ mm/s fitted to the DyN spectrum corresponds to a total efg of $V_{zz} = 30.9(1.1) \times 10^{21}\,{\rm V/m^2}$. Given that the spin-up and spin-down states of the fluctuating doublet are fully stretched, the $4f$ contribution is expected to equal the free-ion value of $V_{zz}^{\rm FI}(Dy^{3+}) = 55.3 \times 10^{21}\,{\rm V/m^2}$ [24]. For an ideal situation with cubic Dy^{3+} site symmetry, there should be zero lattice contribution. However, the difference observed here implies $V_{zz}^{\rm latt} = V_{zz} - {\rm V}_{zz}^{\rm FI} = -24.4(1.1) \times 10^{21}{\rm V/m^2}$ and supports the idea of a distortion along the [100] direction. This will be addressed further in the next section.

The upper two spectra of Fig. 4 were recorded at $T = 80$ and 295 K, well above the Curie temperature, and were therefore analyzed in terms of a pure quadrupole interaction. Moreover, because the asymmetry parameter is zero, the spectra are symmetric and the sign of the quadrupole interaction could not be determined. The fitted parameters are presented in the final two rows of Table II, from which it is immediately evident that the two spectra are very similar. The isomer shifts lie within experimental uncertainty of the value at 5 K, suggesting that the second-order Doppler shift is small. However, the derived efg magnitudes are approximately 43% of their 5 K counterpart. The $4f$ contribution to the efg decreases with increasing temperature and asymptotically reaches zero as the levels of the CF scheme are thermally populated. Given that the quadrupole interaction magnitude is the same at 80 and 295 K, it is most likely that its sign is positive at 77 K, becoming negative at 295 K, as the positive $4f$ efg contribution ($V_{zz}^{4f} > 0$) decreases with temperature and the constant, negative lattice

TABLE III. Crystal field parameters for the Dy^{3+} site in DyN. The Stevens parameters are related to the x and W parameters of Lea *et al.* [25] according to $B_4^0 = Wx/F(4)$ and $B_6^0 = W(1-|x|)/F(6)$ with $F(4) = 60$ and $F(6) = 13860$ for Dy^{3+}.

	B_2^0 (K)	B_4^0 (mK)	B_6^0 (μK)	x	W (K)	Reference
Converted from YbN[a]		−13.37	+43.92	−0.57	+1.40	[26]
PCM (octahedral site)[a,b]		−17.34	+6.09	−0.925	+1.125	
PCM [tetragonal distortion, $\epsilon \approx -0.024(10)$][c]	−1.0(4)					

[a]Adopting $(1-\sigma_n) = 1$ and taking values of θ_n and $\langle r^n\rangle_{4f}$ from Refs. [27] and [28], respectively.
[b]Using Eqs. (6) and (7) with $R = a(\mathrm{DyN})/2 = 2.4505$ Å from Ref. [5].
[c]Using Eq. (8) with $(1-\sigma_2) = 0.646$ and $\langle r^2\rangle_{4f} = 0.67651\, a_0{}^2$.

efg contribution ($V_{zz}^{\mathrm{latt}} \approx -24.4(1.1) \times 10^{21}\mathrm{V/m}^2$) becomes increasingly dominant.

IV. CRYSTAL FIELD CONSIDERATIONS

An intriguing outcome of the ^{161}Dy Mössbauer measurements is that the CF ground state for Dy^{3+} in the DyN sample is essentially fully stretched with $|\langle\pm|J_z|\pm\rangle| \approx 15/2$. However, in the ideal rock salt structure, Dy occupies the 4(a) site with cubic point symmetry $m\bar{3}m$. According to the CF scheme systematics for J = 15/2 (Fig. 2 of Ref. [25]), the two doublet ground state possibilities are Γ_6 and Γ_7 with $|\langle\pm|J_z|\pm\rangle|$ values of only 2.5 and 2.83, respectively. Noting that (i) XRD suggests a small tetragonal distortion along the [100] axis and (ii) Mössbauer spectroscopy indicated a nonzero lattice contribution to the efg at the ^{161}Dy nucleus, it is worth exploring the effect of distortion on the Dy^{3+} CF scheme and, in particular, its doublet ground state.

The CF Hamiltonian for cubic point symmetry, with the quantization axis set parallel to the fourfold symmetry [100] axis, is given by

$$\mathcal{H}_{\mathrm{CF}} = B_4^0\{O_4^0 + 5O_4^4\} + B_6^0\{O_6^0 - 21O_6^4\} \qquad (4)$$

where only the two independent CF parameters B_4^0 and B_6^0 are required. It appears that the sole experimental CF parameters available are those determined by Kohgi *et al.* [26] for YbN using inelastic neutron scattering (INS). One possibility is therefore to convert these for use with DyN via

$$B_n^0(\mathrm{Dy}^{3+}) = \frac{[\theta_n(1-\sigma_n)\langle r^n\rangle_{4f}]_{\mathrm{Dy}^{3+}}}{[\theta_n(1-\sigma_n)\langle r^n\rangle_{4f}]_{\mathrm{Yb}^{3+}}} \times B_n^0(\mathrm{Yb}^{3+}) \qquad (5)$$

with the multiplying factors θ_n and $4f$ shell radial averages $\langle r^n\rangle_{4f}$ taken from Stevens [27] and Freeman and Desclaux [28], respectively. For the higher ranks with $n = 4$ and 6, the CF shielding factors $(1-\sigma_n)$, are assumed to be close to unity.

Another approach in the literature has been to estimate the CF parameters using the point charge model (PCM) approximation with summation over just the local octahedron of nearest-neighbor nitrogen ions, resulting in the expressions

$$B_4^0 = -\frac{\theta_4(1-\sigma_4)\langle r^4\rangle_{4f}}{4\pi\epsilon_0} \times \frac{7}{16} \times \frac{Z|e|^2}{R^5} \qquad (6)$$

and

$$B_6^0 = -\frac{\theta_6(1-\sigma_6)\langle r^6\rangle_{4f}}{4\pi\epsilon_0} \times \frac{3}{64} \times \frac{Z|e|^2}{R^7} \qquad (7)$$

For the purpose of these calculations, the Dy-N distance was taken as half the bulk cubic lattice parameter of $a = 4.901$Å [5], and the charge adopted for the nitrogen sites was $q_{\mathrm{N}} = Z|e|$ with $Z = -3$ [29]. The CF parameters determined using the above approaches are summarized in the first two rows of Table III, where the estimates for B_4^0 are observed to be in close agreement.

Also included in Table III are the corresponding x (related to the ratio of B_4^0/B_6^0) and W (energy scaling factor) parameters employed in the CF scheme systematics provided by Lea *et al.* [25]. For both sets of CF parameters, the x value falls in the region of the $J = 15/2$ chart, where the Γ_6 doublet is the ground state. The next step was to compute $|\langle\pm|J_z|\pm\rangle|$ for the ground state doublet as a function of an additional B_2^0 term with the z axis set parallel to each of the symmetry directions [100], [111], and [110]. For this purpose, the cubic symmetry parameters converted from YbN [26] were employed. The results are shown in Fig. 5 for $-3\mathrm{K} \leqslant B_2^0 \leqslant +3\mathrm{K}$. Clearly the fully stretched value of $|\langle\pm|J_z|\pm\rangle| = 15/2$ is approached only for the [100] direction and for $B_2^0 \lesssim -2\mathrm{K}$. Finally, the CF energy levels computed as a function of B_2^0 over the range of 0 to −2K are shown in Fig. 6, where it is evident that the low-lying "Γ_6" doublet becomes more and more isolated from the higher levels as B_2^0 increases in magnitude. At 5 K, there would therefore be negligible thermal population of the higher CF doublets, making these conditions ideal for the relaxation model of Nowik and Wickman [15] that was applied in the analysis of the ^{161}Dy Mössbauer spectrum of DyN (Kapton) at $T = 5$ K.

At this point, it is useful to compare the range of $B_2^0 \lesssim -2\mathrm{K}$ predicted above with estimates derived from the experimental XRD and Mössbauer results. First, employing the PCM approach used above [Eqs. (6) and (7)] to estimate B_4^0 and B_6^0, it is straightforward to derive the expression

$$B_2^0 \approx +\frac{\theta_2(1-\sigma_2)\langle r^2\rangle_{4f}}{4\pi\epsilon_0} \times \frac{Z|e|^2}{R^3} \times 3\epsilon \qquad (8)$$

and evaluate B_2^0 corresponding to the XRD determination of the tetragonal distortion ϵ. Second, based on the Mössbauer spectroscopy results for $T = 5$ K, the lattice contribution to the efg at the ^{161}Dy nucleus is equal to $V_{zz}^{\mathrm{latt}} \approx -24.4(1.1) \times 10^{21}\mathrm{V/m}^2$. In the context of the PCM approximation and assuming no other contributions, V_{zz}^{latt} is given by

$$V_{zz}^{\mathrm{latt}} = -\frac{4(1-\gamma_\infty)}{|e|(1-\sigma_2)\langle r^2\rangle_{4f}} \times \frac{B_2^0}{\theta_2} \qquad (9)$$

[30] so that the inverse of this expression can be used to estimate B_2^0. For rank $n = 2$, the CF shielding factor $(1-\sigma_2)$ drops to around 0.5 and needs to be taken into account.

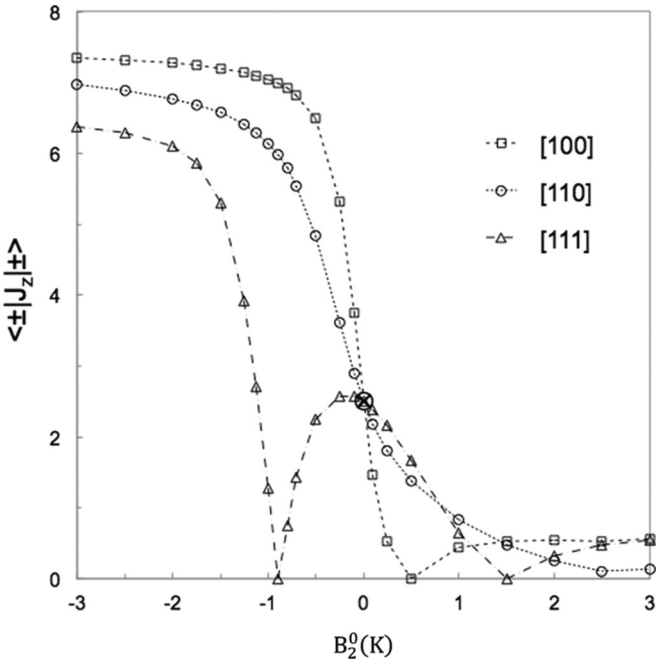

FIG. 5. Expectation value $|\langle\pm|J_z|\pm\rangle|$ for the ground state doublet of the CF scheme for Dy^{3+} ($J = 15/2$) in DyN as a function of an additional B_2^0 term with the z axis set parallel to each of the symmetry directions [100], [111], and [110]. The fully stretched value of $|\langle\pm|J_z|\pm\rangle| = 15/2$ is approached only for the [100] direction and with $B_2^0 \lesssim -2$ K. The cubic symmetry CF parameters of $B_4^0 = -13.37$ mK and $B_6^0 = +43.92\,\mu$K (fourfold symmetry axis representation) were converted from inelastic neutron scattering results reported for YbN [26].

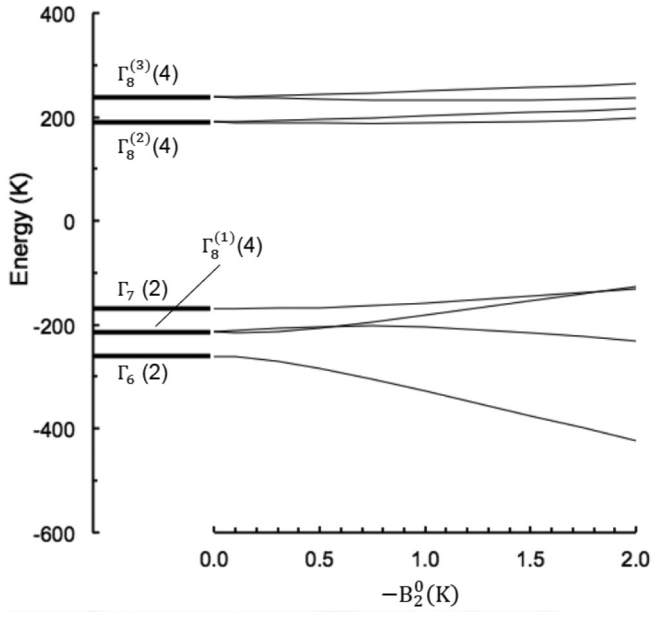

FIG. 6. Crystal field scheme (left) for the cubic Dy^{3+} ion site of DyN based on the parameters of $B_4^0 = -13.37$ mK and $B_6^0 = +43.92\,\mu$K ($x = -0.57$, $W = +1.40$ K in the convention of Lea *et al.* [25]) converted from inelastic neutron scattering results reported for YbN [26]. The right-hand section of the figure shows the influence on the energy levels of a negative B_2^0 term with increasing magnitude.

Using values of $(1 - \sigma_2) = 0.646$, $\langle r^2\rangle_{4f} = 0.67651\,a_0{}^2$, and $(1 - \gamma_\infty) = 60.97$ from Gupta and Sen [31] and $\theta_2 = -0.006349$ from Stevens [27], the lattice distortion approach [Eq. (8)] yields $B_2^0 = -1.0(4)$K, and the lattice efg conversion approach [Eq. (9)] gives $B_2^0 = -3.9(2)$K. These results provide broad support for tetragonal distortion corresponding to an induced $B_2^0 \lesssim -2$K. However, there are limitations to these two approaches. Even for cases where the PCM is a good approximation, the summation over point charges converges much more slowly with distance from the central ion for the rank $n = 2$ case than for the higher ranks $n = 4$ and 6. Therefore, the restriction to nearest-neighbor nitrogen ligands in Eq. (8) is a substantial approximation. With regard to Eq. (9), it was pointed out by Coehoorn *et al.* [32] that the shielding factors ignore the contribution of the valence electrons to the electric field gradient and/or the CF parameter. In such circumstances, the ratio $(1 - \gamma_\infty)/(1 - \sigma_2)$ might instead be regarded as a free parameter. For the rare earth sites of the intermetallics $ErNi_5$ and $TmNi_5$, Gubbens *et al.* [33,34] reported increases of 60–70% in the apparent value of $(1 - \gamma_\infty)/(1 - \sigma_2)$ compared with the straightforward substitution of shielding factors from Gupta and Sen [31]. If a similar increase is applied in the present calculation, then Eq. (9) leads to $B_2^0 = -2.4(3)$K.

Finally, we consider how an extended system of the proposed, fully stretched, relaxing doublets would behave magnetically. As a two-level system, it can be assigned the effective spin $S = 1/2$ with $m_S = \pm 1/2$. A value of $g_{\rm eff} = 20$ then provides the full moments of magnitude $|\mu_\pm| = g_{\rm eff} \times 1/2 = 10\ \mu_B/Dy^{3+}$ that were deduced from the ^{161}Dy Mössbauer spectroscopy. It is interesting that this simple approach gives an effective paramagnetic moment of $\mu_{\rm eff} = g_{\rm eff}\sqrt{S(S+1)} = 20\sqrt{\frac{1}{2}(\frac{1}{2}+1)} \approx 17.3\,\mu_B/Dy^{3+}$, slightly larger than the value of $\mu_{\rm eff} = 14.7\,\mu_B/Dy^{3+}$ extracted from the magnetic susceptibility data in Sec. 3.2.

A simple molecular field approach then requires the solution

$$m = \tanh\left(\frac{m}{t}\right) \tag{10}$$

with $m = \langle\mu\rangle/\mu_{\rm sat}$, $\mu_{\rm sat} = 10\,\mu_B$, and $t = T/\theta_C$. In this case, θ_C is an effective Curie-Weiss temperature for the isolated doublet rather than what would be derived from inverse susceptibility data recorded in the paramagnetic state at temperatures sufficient to populate the full set of CF levels. The predicted average moment at 5 K is shown in Fig. 7 as a function of the unknown Curie-Weiss temperature. The corresponding doublet splitting,

$$\Delta = 2k_B\theta_C \tanh\left(\frac{m}{t}\right) \tag{11}$$

is shown in the inset. It is evident from these plots that an effective Curie temperature in the range of $\theta_C =$ 6–7 K would be required to achieve both the splitting of 13(2) K fitted to the Mössbauer data and the saturation moment of close to $4\,\mu_B$ determined from the low temperature magnetization data. This is substantially smaller than the observed Curie temperature of $T_C =$ 17–26 K and implies a weaker magnetic exchange interaction than was expected.

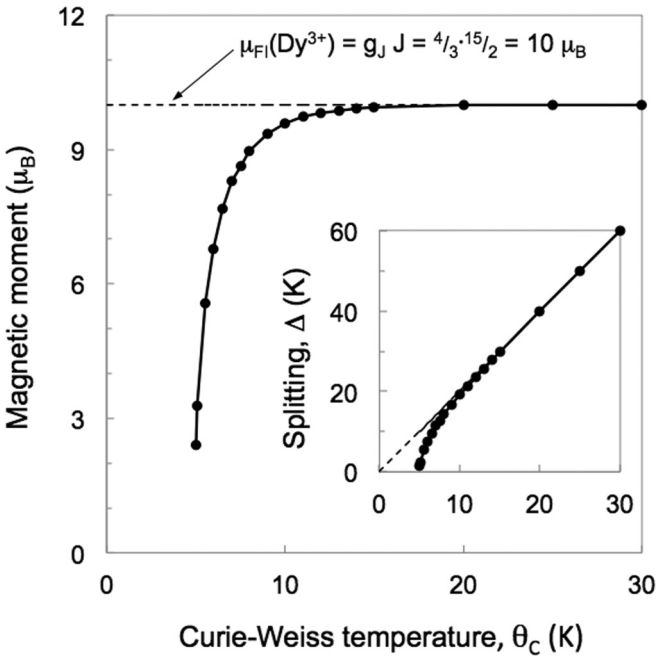

FIG. 7. Average Dy^{3+} moment predicted at $T = 5\,K$ for an isolated fully stretched ground state doublet and shown as a function of the appropriate two-level Curie-Weiss temperature. The associated doublet splitting is shown in the inset.

V. CONCLUDING REMARKS

^{161}Dy Mössbauer spectroscopy was employed to investigate the mechanism responsible for the suppressed magnetic moment of nominally cubic DyN. For this purpose, thick DyN rare earth nitride films were grown on a Kapton organic substrate using IAD. The low temperature ^{161}Dy Mössbauer spectra were consistent with thermal relaxation between fully stretched $\pm 10\,\mu_B$ levels of a low-lying Kramers doublet. Crystal field considerations indicated that this is possible only if an additional rank 2 crystal field term $B_2^0 \approx -2K$ is induced by tetragonal distortion. The XRD data provide some supportive evidence for this conclusion. Considered in isolation, a fluctuating moment of increased magnitude for the low-lying doublet appears to be inconsistent with the observation of a reduced bulk magnetization. However, the tetragonal distortion also leads to greater energy separation of this low-lying doublet from the higher CF levels, resulting in a well-defined two-level magnetic system with an effective spin of $S_{eff} = 1/2$. It is this secondary outcome, in combination with a substantially reduced exchange interaction (or effective Curie-Weiss temperature) for the doublet system that is ultimately responsible for the suppressed magnetic moment of the DyN film. A related treatment was recently employed by Anton *et al.* [29] to account for the bulk magnetization of their thin film (120 nm) NdN specimens. The fact that the DyN thick films investigated in this paper present issues similar to those of much thinner NdN film specimens supports the idea that their properties are driven predominantly by the deposition process. Finally, it is interesting that the concept of a tetragonally distorted rare earth ion environment was hinted at in the earlier theoretical paper of Larson and Lambrecht [35], where it was observed that a lower rare earth site symmetry could lead to a more stable state. We believe that a tetragonal lattice distortion could also apply to other heavy rare earth nitride films that exhibit lower than expected bulk magnetizations.

ACKNOWLEDGMENTS

The authors acknowledge David Cortie (Research School of Chemistry, Australian National University) for useful discussions. J.P.E. gratefully acknowledges his Australian Postgraduate Award. This project received financial support from the Australian Institute of Nuclear Science and Engineering (Grant No. ALNGRA14551) and the University of New South Wales. J.P.E. and J.E.D. acknowledge Peter Ha and Alex Stokes for their assistance at the Australian National Fabrication Facility. J.M.C. and G.A.S. thank the staff at the OPAL reactor in Sydney, where the activation of the ^{161}Dy Mössbauer source was carried out.

[1] F. Natali, B. J. Ruck, N. O. V. Plank, H. J. Trodahl, S. Granville, C. Meyer, and W. R. L. Lambrecht, Rare-earth mononitrides, Prog. Mater. Sci. **58**, 1316 (2013).

[2] R. Didchenko and F. P. Gortsema, Some electric and magnetic properties of rare earth monosulfides and nitrides, J. Phys. Chem. Solids **24**, 863 (1963).

[3] N. Sclar, Properties of rare-earth nitrides, J. Appl Phys. **35**, 1534 (1964).

[4] A. R. H. Preston, S. Granville, D. H. Housden, B. Ludbrook, B. J. Ruck, H. J. Trodahl, A. Bittar, G. V. M. Williams, J. E. Downes, A. DeMasi, Y. Zhang, K. E. Smith, and W. R. L. Lambrecht, Comparison between experiment and calculated band structures for DyN and SmN, Phys. Rev. B **76**, 245120 (2007).

[5] T. Nakagawa, K. Sako, T. Arakawa, and T. A. Yamamoto, Magnetocaloric effect of mononitride containing gadolinium and dysprosium $Gd_xDy_{1-x}N$, J. Alloys Compd. **364**, 53 (2004).

[6] H. R. Child, M. K. Wilkinson, J. W. Cable, W. C. Koehler, and E. O. Wollan, Neutron diffraction investigation of the magnetic properties of compounds of rare-earth metals with group V anions, Phys. Rev. **131**, 922 (1963).

[7] D. L. Cortie, J. D. Browne, S. Bruck, T. Saerbeck, J. P. Evans, H. Fritzsche, X. L. Wang, J. E. Downes, and F. Klose, Intrinsic reduction of the ordered $4f$ magnetic moments in semiconducting rare-earth nitride thin films: DyN, ErN and HoN, Phys. Rev. B **89**, 064424 (2014).

[8] A. A. Moolenaar, A ^{141}Pr Mössbauer Study of Praseodymium Compounds, Doctoral dissertation, Delft University of Technology, 1994.

[9] J. Rodríguez-Carvajal, Recent advances in magnetic structure determination by neutron powder diffraction, Physica B **192**, 55 (1993).

[10] T. Roisnel and J. Rodríguez-Carvajal, WinPLOTR: A windows tool for powder diffraction pattern analysis, Mater. Sci. Forum **378**, 118 (2001).
[11] A. Le Bail, H. Duroy, and J. L. Fourquet, *Ab initio* structure determination of $LiSbWO_6$ by x-ray powder diffraction, Mater. Res. Bull. **23**, 447 (1988).
[12] L. Alexander and H. P. Klug, J. Appl. Phys. **21**, 137 (1950).
[13] P. K. Muduli, A. Pal, and M. G. Blamire, Crossover from diffusive to tunneling regime in NbN-DyN-NbN ferromagnetic semiconductor tunnel junctions, Phys. Rev. B **89**, 094414 (2014).
[14] S. Granville, B. J. Ruck, F. Budde, A. Koo, D. J. Pringle, F. Kuchler, A. R. H. Preston, D. H. Housden, N. Lund, A. Bittar, G. V. M. Williams, and H. J. Trodahl, Semiconducting ground state of GdN thin films, Phys. Rev. B **73**, 235335 (2006).
[15] I. Nowik and H. H. Wickman, Relaxation Phenomena in Mössbauer Spectra of Magnetically Ordered Erbium Ions in $ErFeO_3$, Phys. Rev. Lett. **17**, 949 (1966).
[16] G. J. Bowden, R. K. Day, and P. Martinson, Magnetic anisotropy and the Mössbauer effect in^{161}Dy, J. Phys. F **8**, 2051 (1978).
[17] Y. Berthier, J. Barak, and B. Barbara, NMR of Dy nuclei in ferromagnetic $DyAl_2$ and Dy metal, Solid State Commun. **17**, 153 (1975).
[18] S. Kobayashi, N. Sano, and J. Itoh, NMR measurement of internal field and electric quadrupole interaction in ferromagnetic Dy metal, J. Phys. Soc. Jpn. **21**, 1456 (1966).
[19] J. Tappert, W. Keune, R. A. Brand, P. Vulliet, J.-P. Sanchez, and T. Shinjo, Magnetism and structure of Dy/Fe multilayers studied by ^{57}Fe and ^{161}Dy Mossbauer spectroscopy, J. Appl. Phys. **80**, 4503 (1996).
[20] T. P. Abele, W. G. Bos, and P. J. Ouseph, ^{161}Dy isomer shifts in dysprosium compounds, J. Phys. Chem. Solids **30**, 2159 (1969).
[21] J. Pszczoła, J. Zukrowski, J. Suwalski, and A Pańta, ^{161}Dy and ^{57}Fe Mössbauer effect studies of $Dy[(Fe_{0.4}Co_{0.6})_{1-x}Mn_x]_2$ intermetallics, J. Alloys Compd. **306**, 56 (2000).
[22] M. Belakhovsky, J. Chappert, and D. Schmitt, Mössbauer spectroscopy and magnetic properties of DyMg and ErMg, J. Phys. C: Solid State Phys. **10**, L493 (1977).
[23] P. Raghavan, Table of nuclear moments, At. Data Nucl. Data Tables **42**, 189 (1989).
[24] G. A. Stewart, Some applications of rare-earth Mossbauer spectroscopy, Mater. Forum **18**, 177 (1994).
[25] K. R. Lea, M. J. M. Leask, and W. P. Wolf, The raising of angular momentum degeneracy of f-electron terms by cubic crystal fields, J. Phys. Chem. Solids **23**, 1381 (1962).
[26] M. Kohgi, K. Ohoyama, A. Oyamada, T. Suzuki, and M. Arai, Crystal field excitations in Yb monopnictides, Physica B **163**, 625 (1990).
[27] K. W. H. Stevens, Matrix elements and operator equivalents connected with the magnetic properties of rare earth ions, Proc. Phys. Soc. A **65**, 209 (1952).
[28] A. J. Freeman and J. P. Desclaux, Dirac-Fock studies of some electronic properties of rare-earth ions, J. Magn. Magn. Mater. **12**, 11 (1979).
[29] E.-M. Anton, J. F. McNulty, B. J. Ruck, M. Suzuki, M. Mizumaki, V. N. Antonov, J. W. Quilty, N. Strickland, and H. J. Trodahl, NdN: An intrinsic ferromagnetic semiconductor, Phys. Rev. B **93**, 064431 (2016).
[30] G. A. Stewart, On the interpretation of nuclear quadrupole interaction data for rare-earth nuclei at low symmetry sites, Hyp. Interact. **23**, 1 (1985).
[31] R. P. Gupta and S. K. Sen, Sternheimer shielding–antishielding; rare earth ions, Phys. Rev. A **7**, 850 (1973).
[32] R. Coehoorn, K. H. J. Buschow, M. W. Dirken, and R. C. Thiel, Valence-electron contributions to the electric-field gradient in hcp metals and at Gd nuclei in intermetallic compounds with the $ThCr_2Si_2$ structure, Phys. Rev. B **42**, 4645 (1990).
[33] P. C. M. Gubbens, A. M. van der Kraan, and K. H. J. Buschow, Spin lattice relaxation in $TmNi_5$ above its Curie temperature, J. Magn. Magn. Mater. **50**, 199 (1985).
[34] P. C. M. Gubbens, A. M. van der Kraan, and K. H. J. Buschow, Determination of physical parameters in $4f$-$3d$ intermetallics by rare earth Mössbauer spectroscopy, Hyp. Interact. **50**, 685 (1989).
[35] P. Larson and W. R. L. Lambrecht, Electronic structure of rare-earth nitrides using the LSDA + U approach: Importance of allowing $4f$ orbitals to break the cubic crystal symmetry, Phys. Rev. B **75**, 045114 (2007).